Extracting transport channel transmissions in scanning tunneling microscopy using superconducting excess current

Jacob Senkpiel,[1] Robert Drost,[1] Jan C. Klöckner,[2,3] Markus Etzkorn,[4] Joachim Ankerhold,[5] Juan Carlos Cuevas,[6] Fabian Pauly,[7] Klaus Kern,[1,8] and Christian R. Ast[1,*]

[1]*Max-Planck-Institut für Festkörperforschung, Heisenbergstraße 1, 70569 Stuttgart, Germany*
[2]*Okinawa Institute of Science and Technology Graduate University, Onna-son, Okinawa 904-0495, Japan*
[3]*Fachbereich Physik, Universität Konstanz, 78457 Konstanz, Germany*
[4]*Institut für Angewandte Physik, TU Braunschweig, Mendelssohnstraße 2, 38106 Braunschweig, Germany*
[5]*Institute for Complex Quantum Systems, University of Ulm, Albert-Einstein-Allee 11, 89069 Ulm, Germany*
[6]*Departamento de Física Teórica de la Materia Condensada and Condensed Matter Physics Center (IFIMAC), Universidad Autónoma de Madrid, 28049 Madrid, Spain*
[7]*Institute of Physics, University of Augsburg, 86135 Augsburg, Germany*
[8]*Institut de Physique, École Polytechnique Fédérale de Lausanne, 1015 Lausanne, Switzerland*

(Received 2 August 2021; revised 10 January 2022; accepted 8 March 2022; published 1 April 2022)

Transport through quantum coherent conductors, such as atomic junctions, is described by conduction channels. Information about the number of channels and their transmissions can be extracted from various sources, such as multiple Andreev reflections, dynamical Coulomb blockade, or shot noise. We complement this set of methods by introducing the superconducting excess current as a new tool to continuously extract the transport channel transmissions of an atomic scale junction in a scanning tunneling microscope. In conjunction with *ab initio* simulations, we employ this technique in atomic aluminum junctions to determine the influence of the structure adjacent to the contact atoms on the transport properties.

DOI: 10.1103/PhysRevB.105.165401

I. INTRODUCTION

At the heart of the modern theory of quantum transport lies the concept of transport channels [1,2]. Similar to transverse electromagnetic modes in an optical waveguide, charge can be transported between two baths through a set of distinct pathways arising from individual quantum states. These quantum states are rooted in the electronic structure of a device and can be manipulated by changes in materials or geometry [3]. Each transport channel is further characterized by a transmission value, which specifies the probability for an electron that enters the channel from one bath to be transmitted through it to reach the other bath. The number of transport channels and their respective transmissions, often referred to as the mesoscopic PIN code (in analogy to the personal identification number), characterize a transport configuration.

Established techniques to measure the channel transmissions (mesoscopic PIN code) are either technically challenging (shot-noise measurements) [4–14], time consuming (dynamical Coulomb blockade [15] or multiple Andreev reflection measurements [16–25]), or only applicable to ensemble averages (conductance fluctuations [26,27]). It is, thus, difficult to track the continuous evolution of the channel transmissions as a function of an experimental control parameter to gain deeper insights into the transport process.

In this article, we show that, if, at least, one of the electrodes involved in transport is superconducting, the excess current can be used to determine the channel transmissions in a simple and rapid fashion. Using an ultra-low-temperature scanning tunneling microscope (STM), we study transport properties of superconducting tunnel junctions from the deep tunneling regime to atomic contact and extract the channel transmissions as a continuous function of the junction conductance. By using *ab initio* transport calculations, we are able to elucidate the microscopic nature of the conduction channels.

II. THE EXCESS CURRENT AS A TOOL FOR QUANTUM TRANSPORT

In addition to quasiparticle tunneling, superconducting contacts support another mode for charge transport through Andreev reflections [28]. An electron incident onto the superconductor is reflected as a hole, thereby, transferring a charge of $2e$ into the superconductor and forming a Cooper pair. Higher orders of this process occur in superconductor-superconductor junctions and are referred to as multiple Andreev reflections (MARs).

Even at bias voltages V outside of the superconducting gap ($eV \gg 2\Delta$), the lowest-order Andreev reflection continues to contribute to the current leading to a constant offset from the expected single-particle current [29–31]. Formally, this excess

*Corresponding author: c.ast@fkf.mpg.de

current is defined as

$$I_{\mathrm{exc}} = I_{\mathrm{S}}(V) - I_{\mathrm{N}}(V)|_{eV \gg 2\Delta}, \tag{1}$$

where Δ is the superconducting gap parameter, the subscripts S and N refer to the superconducting and normal states, respectively, and e is the elementary charge. A nonlinear dependence of the excess current on the channel transmission allows an extraction of the junction channel transmissions. Assuming $\Delta_{\mathrm{Tip}} = \Delta_{\mathrm{Sample}} = \Delta$, the excess current across a superconductor-insulator-superconductor junction at zero temperature can be calculated as

$$I_{\mathrm{exc}} = \frac{2e\Delta}{h} \sum_i \frac{\tau_i^2}{1-\tau_i} \left[1 - \frac{\tau_i^2}{2(2-\tau_i)\sqrt{1-\tau_i}} \times \ln\left(\frac{1+\sqrt{1-\tau_i}}{1-\sqrt{1-\tau_i}} \right) \right], \tag{2}$$

where τ_i is the transmission of the ith electronic transport channel and h is Planck's constant [3]. We assume that the τ_is are independent of each other and of the bias voltage V, which is a good approximation in the small energy window around zero bias relevant to transport in atomic contacts. As can be seen from Eq. (2), the excess current depends on the τ_i and Δ but not on the bias voltage V applied to the contact. If only few open transport channels are present, a single data point is, thus, enough to fully determine the channel transmissions, greatly facilitating and expediting data acquisition.

All measurements are performed in a custom-built STM placed in a dilution refrigerator and operating at a base temperature of 10 mK [32]. The Al(100) sample was cleaned by bombardment with Ar ions followed by stepwise annealing in UHV from 480 °C to 460 °C to 435 °C. We extracted individual Al atoms from the substrate and placed them on the pristine Al(100) surface to create a simple transport configuration which serves as a model system for our channel transmissions analysis [33].

We approach the adatom with the STM tip to measure conductance spectra at constant height and $I(z)$ curves. The situation is schematically shown in Fig. 1(a). Conductance spectra acquired at low conductance show the characteristic signature of superconductor-superconductor tunneling with an energy gap around zero bias, flanked by coherence peaks on either side [see Fig. 1(b)]. The values of Δ for tip and sample, required for a quantitative analysis based on Eq. (2) or numerical simulations, can be extracted from a fit as described, for example, in Refs. [34,35]. For the present case in Fig. 1(b), we find $\Delta = 180$ μeV.

Junctions, such as the one described here have been reported to exhibit exceptional stability [35]. Figure 1(c) shows the height-dependent normal-state conductance G_{N} of a typical junction calculated from an $I(z)$ measurement at 1.5 mV, outside the gap, in units of the quantum of conductance $G_0 = 2e^2/h$. We define the point $z = 0$ to be at the maximum of conductance. At first, the conductance increases exponentially at a rate of roughly one order of magnitude per 100 pm as expected from theory until reaching a maximum value near G_0. If the tip is approached further, the conductance decreases at a rate which depends on the microtip. In some cases, a reduction to about $0.2G_0$ has been observed. Remarkably, no jump to contact occurs [36], and there is no hysteresis in the current when retracting the tip [33]. We conclude that the junction remains unchanged after the approach-retract cycle.

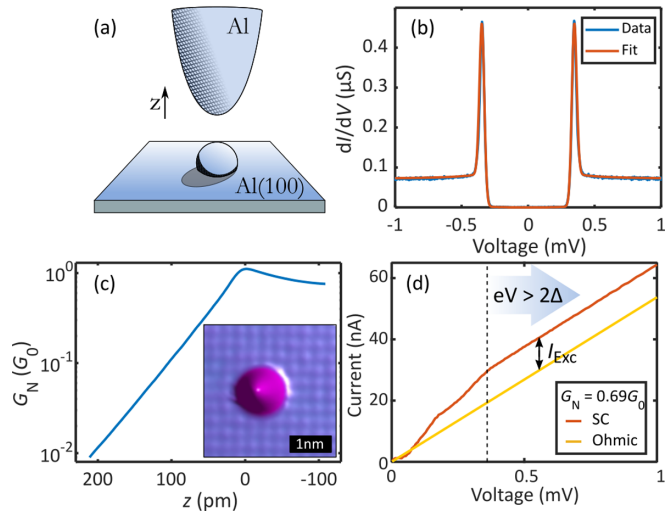

FIG. 1. (a) Sketch of the single-atom junction studied in the experiment. The tip height z is adjusted in the course of the experiment. (b) Quasiparticle spectrum at low set-point conductance (blue) with corresponding fit. (c) Conductance curve $G_{\mathrm{N}}(z)$ recorded above an Al adatom, showing a clear initial exponential increase of the conductance (set-point 1.5 mV at 1 nA). The inset: Topographic image of an Al adatom on the Al(100) surface. (d) $I(V)$ curve of the superconducting sample at $G_{\mathrm{N}} = 0.69G_0$. The currents in the superconducting state (red, SC) and in the normal state (yellow, Ohmic) correspond to the currents $I_{\mathrm{S,N}}$ in Eq. (1), respectively. The excess current is the y-axis intercept of the curve at $eV > 2\Delta$. The dashed vertical line indicates $2\Delta = 360$ μeV.

Although the general shape of the height-dependent conductance is consistent across measurements with different microtips, the value of the maximum conductance $G_{\mathrm{N}}^{\mathrm{max}}$ attained and the magnitude of the drop past $G_{\mathrm{N}}^{\mathrm{max}}$ varies significantly [33]. These differences must be rooted in the details of quantum transport between tip and sample as characterized by the channel transmissions. Monitoring the channel transmissions continuously as a function of z promises deeper insights into the quantum properties of the junctions.

As can be seen from Eq. (2), the complete information about the channel transmissions is contained in the excess current. The $I(V)$ characteristic of a superconducting tunnel junction evolves to first order in V for $eV > 2\Delta$, but it does not pass through the origin. It instead intersects the current axis at a constant value, referred to as the excess current [see Fig. 1(d)]. It arises from the lowest-order Andreev reflection, which contributes to the total current even outside the gap. Indeed, an established method of extracting the channel transmissions is to analyze the subharmonic gap structure due to MARs in a superconducting junction at high conductance. MARs lead to a series of features at integer fractions of 2Δ, which characterize the channel configuration. The excess current, having the same physical origin, contains identical information.

To show that an analysis of the excess current is a pertinent way of determining the junction channel transmissions,

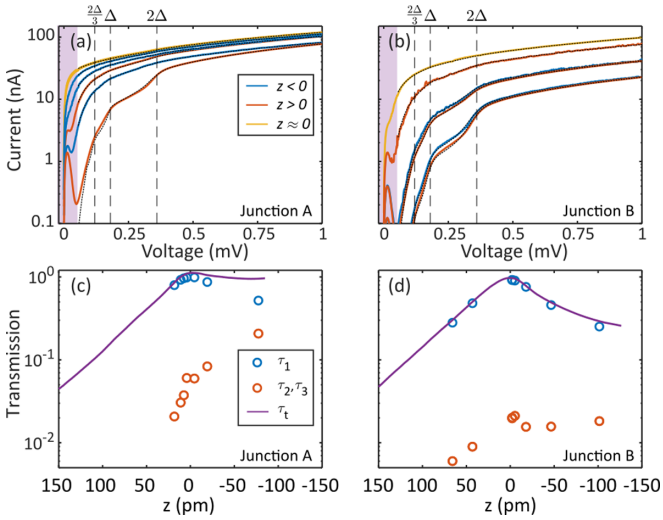

FIG. 2. (a) and (b) $I(V)$ curves at various conductances for two typical Al adatoms. MARs appear as steps in the current at fractions of 2Δ. Fits to the data are superimposed on black dotted lines. The shaded areas for small voltages ($V < 50\ \mu$V) are excluded from the analysis due to the presence of the Josephson current. (c) and (d) Channel transmission analysis from the MAR model for the junctions in panels (a) and (b), respectively, as circles. The purple curve shows the total transmission, i.e. the conductance $G_N(z)$ in units of G_0.

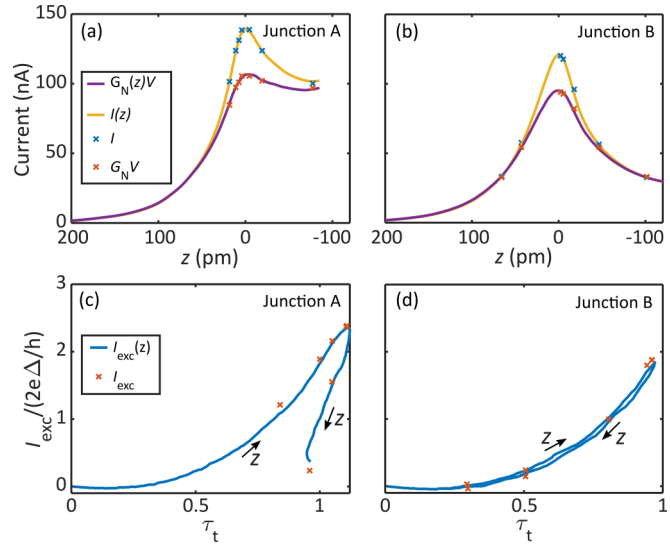

FIG. 3. (a) and (b) Measured current (yellow) and reconstructed $G_N(z)V$ (purple) signals for junctions A and B, respectively. The difference between the two curves results from the excess current. The blue and orange crosses show the same quantities from the MAR point spectra in Figs. 2. (c), (d) Excess current (blue lines) as a function of total transmission τ_t for junctions A and B, respectively. The crosses ($\times$) indicate the excess current independently extracted from the corresponding MAR analysis for comparison. Note that the curves show the approach curve of the tip, i.e., the arrows indicate the direction of decreasing z.

we supplement our continuous $I(z)$ measurements of the excess current with full MAR spectra at selected points in the $I(z)$ curve. Representative data sets from two distinct junctions are shown in Figs. 2(a) and 2(b). The superconducting gap is visible as a step in the $I(V)$ curve at $2\Delta = 360\ \mu$eV, whereas the MARs are manifested as shoulders at $eV = 2\Delta/2,\ 2\Delta/3, \ldots$. In addition to the MARs, the Josephson effect, the coherent tunneling of Cooper pairs, is visible as a sharp rise in current close to zero bias. Strong z-dependent variations of the subgap structure are clearly apparent in both data sets, pointing towards changes in the channel configuration.

We use a well-established model based on the relation between MARs and channel transmissions [37,38] to analyze the channel configuration of the different junctions and their dependence on the total transmission. Owing to its partially filled p shell, we assume that an atomic contact of Al may sustain up to three distinct transport channels. Due to this construction, we find the two transport channels having π symmetry to be degenerate. We fit the MAR data using values for Δ and the Dynes broadening parameter [39], which we both extract from a quasiparticle fit, such as the one shown in Fig. 1(b), and capture the environmental broadening by a convolution with a Gaussian [35]. The voltage range between $\pm 50\ \mu$V, dominated by Josephson transport, is excluded from the analysis. The results of this channel analysis are presented in Figs. 2(c) and 2(d). The nonlinear dependence of the different orders of Andreev reflections on the channel transmissions allows us to extract their values. Comparing this with the total conductance, which is well reproduced by our calculations, we confirm the predominant single-channel nature of the contacts.

We now turn toward the task of extracting the excess current from the $I(z)$ traces. As can be seen from Fig. 1(d), the excess current may be regarded as an integration constant when calculating the current from conductance. We define the normal-state current at bias voltage V as

$$I_N(z) = G_N(z)V, \tag{3}$$

where G_N is the differential conductance which is measured directly by means of a lock-in amplifier at a high bias voltage outside of the superconducting gap. Equivalently, the differential conductance can be extracted from the slope of the $I(V)$ curve at high bias voltage. The excess current is then the difference between the experimentally detected current and the normal-state current, see Eq. (1).

Representative results from the excess current determination are shown in Fig. 3 for the same two junctions which have been discussed in the context of Fig. 2. Figures 3(a) and 3(b) show the experimentally measured current in yellow and the calculated normal-state current according to Eq. (3) in purple. The blue and orange markers show the same quantities as derived from the spectra shown in Figs. 2(a) and 2(b). The excess current itself is plotted in Figs. 3(c) and 3(d). The behavior of I_{exc} is starkly different for both junctions. Although I_{exc} decreases sharply past the point of maximum conductance in junction A, it is nearly symmetric around the point of maximum conductance in junction B. We will now show that the source of these differences lies in the height-dependent evolution of the channel transmissions of both junctions.

Combining this with the total conductance, which is the sum of the transmissions of all channels, we can determine the

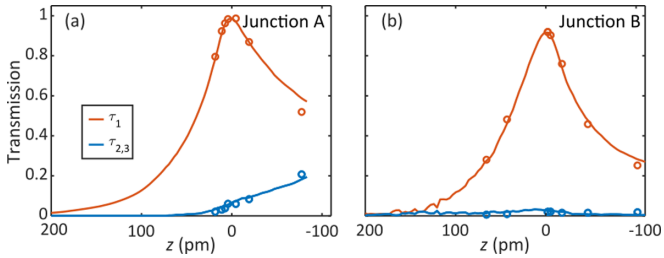

FIG. 4. (a) and (b) Channel transmission analysis using the excess current for junctions A and B, respectively, with the dominant channel in orange and the degenerate channels shown in blue. The circles show the result of the full MAR analysis from Fig. 2.

transmissions of up to two independent transport channels (or three channels if two of them are degenerate as in our case) in the low conductance regime in analogy to shot-noise measurements [6–14]. At higher conductance and higher individual channel transmissions, the excess current depends on a higher-order polynomial ($n > 2$) of the τ_i so that the transmissions of more than two channels can be extracted simultaneously [17,18]. Figure 4 shows the resulting transmissions τ_i for the dominant (orange) and degenerate (blue) channels for junctions A and B. As a control, the results of the full MAR analysis are superimposed as open circles. The analysis of the excess current finds virtually the same channel configuration as the established MAR analysis at those points where data from both methods are available. This agreement is expected since the physical processes at the heart of both methods are the same. The measurement can, hence, be simplified from a full $I(V)$ characteristic to a single data point with no apparent loss of accuracy.

Owing to the ease and speed of the measurement, the excess current provides a very refined picture of the channel evolution as a function of z. In general, the dominant channel increases as the tip is approached until reaching nearly unity transmission at which point τ_1 drops sharply. The transparency of the secondary channels, when present, increases rather monotonously for smaller z. A similar drop in the total transmission has been observed in Al junctions before and was attributed to varying channel transmissions under elastic deformation of the contact [40]. A comparatively detailed decomposition into individual transport channels as we report here has not been achieved until now.

To understand the observed channel transmission variations between different junctions and to tie them to microscopic origins, we performed *ab initio* simulations using density functional theory (DFT) for two microtips terminated by a (100) and a (111) facet, facing a Al(100) surface with a tip atom on top. The junction geometries are optimized at each tip height, and their transport characteristics, including the transmission channels, are computed from the electronic structure through nonequilibrium Green's function (NEGF) technique [33,41]. The channel transmissions obtained from the simulations of the two different tips are shown in Figs. 5(a) and 5(b).

The simulations qualitatively reproduce the experimental observations with the total conductance reaching a maximum value and, subsequently, decreasing upon closer approach.

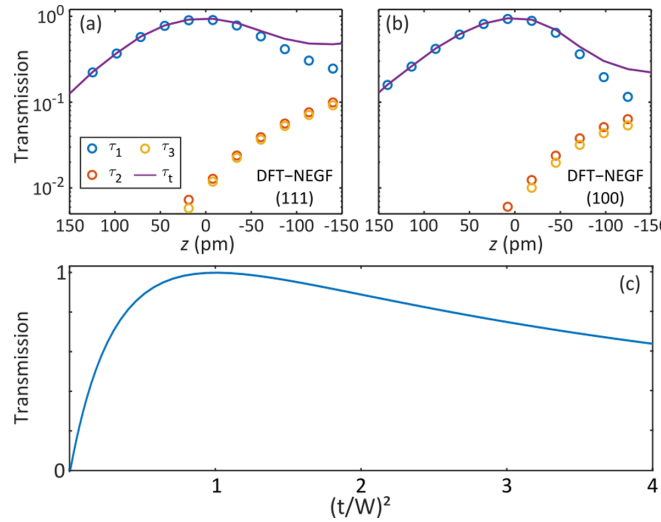

FIG. 5. (a) and (b) Calculated channel transmissions for a (111) and a (100) terminated tip, respectively, above an Al adatom on Al(100) as a function of tip-sample separation. (c) Transmission through two coupled chains according to Eq. (4). The model qualitatively reproduces the experimental data.

The magnitude of the drop-off is dependent on the crystal facet exposed by the tip. As it is unlikely that the tip apex in the experiment is perfectly crystalline, an exact reproduction of the experimental data is not expected. It is clear, although, that changes in the evolution of the channel transmissions can be traced to structural properties of the microtip.

The DFT simulations also allow us to extract the coupling strength between the tip and the sample electrodes, which rises continuously as a function of z. The rise does not necessarily translate into a higher transmission though. This behavior can be qualitatively understood in a one-dimensional tight-binding model. We, thus, study two semi-infinite atomic chains with uniform nearest-neighbor hopping amplitude t_0, and coupled to each other by the hopping t. In the limit $t \ll t_0$, itinerant charges in the chain are likely to be back-scattered from the point of contact. In the other limiting case $t \gg t_0$, electrons are likely to pass back and forth between the two sides of the junction, thereby, blocking it for transport. This kind of system has been described theoretically in Ref. [3]. The transmission is

$$\tau = \frac{4t^2/W^2}{(1 + t^2/W^2)^2}, \tag{4}$$

where t is the coupling between the two semi-infinite chains and $W = 1/[\pi\rho(E_F)]$ is an energy scale related to the density of states at the Fermi level. This model allows us to understand the essential physics of single atom tunnel junctions in a minimal setting. In the weak-coupling limit, the small interchain hopping acts as a potential barrier that limits the charge transfer between the two leads. However, when the interchain coupling becomes larger than the intrachain hopping, a bound state forms between the leads, which also inhibits charge transfer. These predictions are in qualitative agreement with our experimental results, see Fig. 5(c).

III. CONCLUSIONS

The channel transmissions are the central quantity for understanding quantum transport in mesoscopic contacts. They are a general property of a transport configuration and do not change between the superconducting and the normal states. When, at least, one of the electrodes participating in transport is superconducting, the channel transmissions can be derived from Andreev processes. The excess current has its origin in MARs, which continue to contribute to the total current even as $eV > 2\Delta$. It, therefore, contains the same physical information as the subgap structure, whereas being both easier and faster to measure.

To summarize, we use the excess current to measure the continuous evolution of the channel transmissions in tunnel junctions. Control experiments using a full MAR analysis confirm the accuracy of our procedure. The ability to extract complex quantum properties such as the channel transmissions from such a simple measurement holds the promise of understanding transport as a function of an external control parameter or to relate atomic structure to transport in much greater detail than hitherto possible.

ACKNOWLEDGMENTS

This work was funded, in part, by the ERC Consolidator Grant AbsoluteSpin (Grant No. 681164). J.C.K. and F.P. thank the Collaborative Research Center (SFB) 767 of the German Research Foundation (DFG) as well as the Okinawa Institute of Science and Technology (OIST) Graduate University for financial support. Part of the numerical modeling was performed using the computational resources of the BWHPC program, namely, the bwUniCluster and the JUSTUS HPC facility. J.C.C. acknowledges funding from the Spanish Ministry of Science and Innovation (Grant No. PID2020-114880GB-I00). J.A. acknowledges funding from the Center for Integrated Quantum Science & Technology (IQ^{ST}) and the DFG through AN336/13-1.

[1] R. Landauer, Spatial variation of currents and fields due to localized scatterers in metallic conduction, IBM J. Res. Dev. **1**, 223 (1957).

[2] R. Landauer, Electrical resistance of disordered one-dimensional lattices, Philos. Mag. **21**, 863 (1970).

[3] J. C. Cuevas, Electronic transport in normal and superconducting nanostructures, Ph.D. thesis, Universidad Autónoma de Madrid, 1999.

[4] H. E. van den Brom and J. M. van Ruitenbeek, Quantum Suppression of Shot Noise in Atom-Size Metallic Contacts, Phys. Rev. Lett. **82**, 1526 (1999).

[5] R. J. Schoelkopf, P. J. Burke, A. A. Kozhevnikov, D. E. Prober, and M. J. Rooks, Frequency Dependence of Shot Noise in a Diffusive Mesoscopic Conductor, Phys. Rev. Lett. **78**, 3370 (1997).

[6] Y. Blanter and M. Büttiker, Shot noise in mesoscopic conductors, Phys. Rep. **336**, 1 (2000).

[7] R. Cron, M. F. Goffman, D. Esteve, and C. Urbina, Multiple-Charge-Quanta Shot Noise in Superconducting Atomic Contacts, Phys. Rev. Lett. **86**, 4104 (2001).

[8] N. Agraït, A. L. Yeyati, and J. M. van Ruitenbeek, Quantum properties of atomic-sized conductors, Phys. Rep. **377**, 81 (2003).

[9] D. Djukic and J. M. van Ruitenbeek, Shot noise measurements on a single molecule, Nano Lett. **6**, 789 (2006).

[10] M. Kumar, O. Tal, R. H. M. Smit, A. Smogunov, E. Tosatti, and J. M. van Ruitenbeek, Shot noise and magnetism of Pt atomic chains: Accumulation of points at the boundary, Phys. Rev. B **88**, 245431 (2013).

[11] R. Vardimon, M. Klionsky, and O. Tal, Experimental determination of conduction channels in atomic-scale conductors based on shot noise measurements, Phys. Rev. B **88**, 161404(R) (2013).

[12] A. Burtzlaff, A. Weismann, M. Brandbyge, and R. Berndt, Shot Noise as a Probe of Spin-Polarized Transport through Single Atoms, Phys. Rev. Lett. **114**, 016602 (2015).

[13] R. Vardimon, M. Klionsky, and O. Tal, Indication of complete spin filtering in atomic-scale nickel oxide, Nano Lett. **15**, 3894 (2015).

[14] R. Vardimon, M. Matt, P. Nielaba, J. C. Cuevas, and O. Tal, Orbital origin of the electrical conduction in ferromagnetic atomic-size contacts: Insights from shot noise measurements and theoretical simulations, Phys. Rev. B **93**, 085439 (2016).

[15] J. Senkpiel, J. C. Klöckner, M. Etzkorn, S. Dambach, B. Kubala, W. Belzig, A. L. Yeyati, J. C. Cuevas, F. Pauly, J. Ankerhold, C. R. Ast, and K. Kern, Dynamical Coulomb Blockade as a Local Probe for Quantum Transport, Phys. Rev. Lett. **124**, 156803 (2020).

[16] C. J. Muller, J. M. van Ruitenbeek, and L. J. de Jongh, Experimental observation of the transition from weak link to tunnel junction, Physica C **191**, 485 (1992).

[17] E. Scheer, P. Joyez, D. Esteve, C. Urbina, and M. H. Devoret, Conduction Channel Transmissions of Atomic-Size Aluminum Contacts, Phys. Rev. Lett. **78**, 3535 (1997).

[18] E. Scheer, N. Agraït, J. C. Cuevas, A. Levy Yeyati, B. Ludoph, A. Martín-Rodero, G. R. Bollinger, J. M. van Ruitenbeek, and C. Urbina, The signature of chemical valence in the electrical conduction through a single-atom contact, Nature (London) **394**, 154 (1998).

[19] M. Chauvin, P. vom Stein, D. Esteve, C. Urbina, J. C. Cuevas, and A. Levy Yeyati, Crossover from Josephson to Multiple Andreev Reflection Currents in Atomic Contacts, Phys. Rev. Lett. **99**, 067008 (2007).

[20] M. L. Della Rocca, M. Chauvin, B. Huard, H. Pothier, D. Esteve, and C. Urbina, Measurement of the Current-Phase Relation of Superconducting Atomic Contacts, Phys. Rev. Lett. **99**, 127005 (2007).

[21] B. Ludoph, N. van der Post, E. N. Bratus, E. V. Bezuglyi, V. S. Shumeiko, G. Wendin, and J. M. van Ruitenbeek, Multiple Andreev reflection in single-atom niobium junctions, Phys. Rev. B **61**, 8561 (2000).

[22] J. Riquelme, L. de la Vega, A. L. Yeyati, N. Agraït, A. Martin-Rodero, and G. Rubio-Bollinger, Distribution of conduction

channels in nanoscale contacts: Evolution towards the diffusive limit, Europhys. Lett. **70**, 663 (2005).

[23] F. Massee, Q. Dong, A. Cavanna, Y. Jin, and M. Aprili, Atomic scale shot-noise using cryogenic MHz circuitry, Rev. Sci. Instrum. **89**, 093708 (2018).

[24] F. Massee, Y. K. Huang, M. S. Golden, and M. Aprili, Noisy defects in the high-T_c superconductor $Bi_2Sr_2CaCu_2O_{8+x}$, Nat. Commun. **10**, 544 (2019).

[25] K. M. Bastiaans, T. Benschop, D. Chatzopoulos, D. Cho, Q. Dong, Y. Jin, and M. P. Allan, Amplifier for scanning tunneling microscopy at MHz frequencies, Rev. Sci. Instrum. **89**, 093709 (2018).

[26] B. Ludoph, M. H. Devoret, D. Esteve, C. Urbina, and J. M. van Ruitenbeek, Evidence for Saturation of Channel Transmission from Conductance Fluctuations in Atomic-Size Point Contacts, Phys. Rev. Lett. **82**, 1530 (1999).

[27] B. Ludoph and J. M. van Ruitenbeek, Conductance fluctuations as a tool for investigating the quantum modes in atomic-size metallic contacts, Phys. Rev. B **61**, 2273 (2000).

[28] A. Andreev, The thermal conductivity of the intermediate state in superconductors, Zh. Eksp. Teor. Fiz. **46**, 1823 (1964) [Sov. Phys. JETP **19**, 1228 (1964)].

[29] S. N. Artemenko, A. F. Volkov, and A. V. Zaitsev, On the excess current in microbridges S-c-S and S-c-N, Solid State Commun. **30**, 771 (1979).

[30] A. V. Zaitsev, Theory of pure short S-c-S and S-c-N microjunctions, Zh. Eksp. Teor. Fiz. **78**, 221 (1980), [Sov. Phys. JETP **51**, 111 (1980)].

[31] G. E. Blonder, M. Tinkham, and T. M. Klapwijk, Transition from metallic to tunneling regimes in superconducting microconstrictions: Excess current, charge imbalance, and supercurrent conversion, Phys. Rev. B **25**, 4515 (1982).

[32] M. Assig, M. Etzkorn, A. Enders, W. Stiepany, C. R. Ast, and K. Kern, A 10 mK scanning tunneling microscope operating in ultra high vacuum and high magnetic fields, Rev. Sci. Instrum. **84**, 033903 (2013).

[33] See Supplemental Material at http://link.aps.org/supplemental/10.1103/PhysRevB.105.165401 for additional data and further details on sample preparation, absence of jump to contact, hysteresis in approach-retract curves, and DFT-NEGF simulations. See also Refs. [42–45] therein.

[34] C. R. Ast, B. Jäck, J. Senkpiel, M. Eltschka, M. Etzkorn, J. Ankerhold, and K. Kern, Sensing the quantum limit in scanning tunneling spectroscopy, Nat. Commun. **7**, 13009 (2016).

[35] J. Senkpiel, S. Dambach, M. Etzkorn, R. Drost, C. Padurariu, B. Kubala, W. Belzig, A. L. Yeyati, J. C. Cuevas, J. Ankerhold *et al.*, Single channel Josephson effect in a high transmission atomic contact, Commun. Phys. **3**, 131 (2020).

[36] C. Untiedt, M. J. Caturla, M. R. Calvo, J. J. Palacios, R. C. Segers, and J. M. van Ruitenbeek, Formation of a Metallic Contact: Jump to Contact Revisited, Phys. Rev. Lett. **98**, 206801 (2007).

[37] J. C. Cuevas, A. Martín-Rodero, and A. Levy Yeyati, Hamiltonian approach to the transport properties of superconducting quantum point contacts, Phys. Rev. B **54**, 7366 (1996).

[38] J. C. Cuevas, A. Levy Yeyati, and A. Martín-Rodero, Microscopic Origin of Conducting Channels in Metallic Atomic-Size Contacts, Phys. Rev. Lett. **80**, 1066 (1998).

[39] R. C. Dynes, V. Narayanamurti, and J. P. Garno, Direct Measurement of Quasiparticle-Lifetime Broadening in a Strong-Coupled Superconductor, Phys. Rev. Lett. **41**, 1509 (1978).

[40] J. C. Cuevas, A. Levy Yeyati, A. Martín-Rodero, G. R. Bollinger, C. Untiedt, and N. Agraït, Evolution of Conducting Channels in Metallic Atomic Contacts under Elastic Deformation, Phys. Rev. Lett. **81**, 2990 (1998).

[41] F. Pauly, J. K. Viljas, U. Huniar, M. Häfner, S. Wohlthat, M. Bürkle, J. C. Cuevas, and G. Schön, Cluster-based density-functional approach to quantum transport through molecular and atomic contacts, New J. Phys. **10**, 125019 (2008).

[42] A. Schäfer, C. Huber, and R. Ahlrichs, Fully optimized contracted Gaussian basis sets of triple zeta valence quality for atoms Li to Kr, J. Chem. Phys. **100**, 5829 (1994).

[43] S. G. Balasubramani, G. P. Chen, S. Coriani, M. Diedenhofen, M. S. Frank, Y. J. Franzke, F. Furche, R. Grotjahn, M. E. Harding, C. Hättig, A. Hellweg, B. Helmich-Paris, C. Holzer, U. Huniar, M. Kaupp, A. Marefat Khah, S. Karbalaei Khani, T. Müller, F. Mack, B. D. Nguyen *et al.*, TURBOMOLE: Modular program suite for ab initio quantum-chemical and condensed-matter simulations, J. Chem. Phys. **152**, 184107 (2020).

[44] J. P. Perdew, K. Burke, and M. Ernzerhof, Generalized Gradient Approximation Made Simple, Phys. Rev. Lett. **77**, 3865 (1996).

[45] M. Bürkle, J. K. Viljas, T. J. Hellmuth, E. Scheer, F. Weigend, G. Schön, and F. Pauly, Influence of vibrations on electron transport through nanoscale contacts, Phys. Status Solidi B **250**, 2468 (2013).